Trace metal sorption on nanoplastics: An innovative analytical approach combining surface analysis and mass spectrometry techniques

Antoine Aynard, Cécile Courrèges, Javier Jiménez-Lamana, Anassya Raad, Christelle Miqueu, Bruno Grassl, Stephanie Reynaud

Trace metal sorption on nanoplastics: an innovative analytical approach combining surface analysis and mass spectrometry techniques.

Antoine Aynard[a], Cécile Courrèges*[a], Javier Jiménez-Lamana[a], Anassya Raad[a], Christelle Miqueu[b], Bruno Grassl[a], Stéphanie Reynaud[a]

[a.] *Universite de Pau et des Pays de l'Adour, E2S UPPA, CNRS, IPREM, UMR 5254, Pau, France*

[b.] *Universite de Pau et des Pays de l'Adour, E2S UPPA, CNRS, Laboratoire des Fluides Complexes et leurs Réservoirs - IPRA, UMR 5150, Anglet, France*

*Corresponding author: cecile.courreges@univ-pau.fr

Abstract: The mass and volume concentration of nanoplastics is extremely low, but incredibly high in terms of surface area; this is expected to increase their toxicity through the ab/adsorption and transport of chemical co-pollutants such as trace metals. In this context, we studied the interactions between nanoplastics model materials functionalized with carboxylated groups, with either smooth or raspberry-like surface morphologies, and copper as representative of trace metals. For this purpose, a new methodologie, using two complementary surface analysis techniques: Time-of-Flight Secondary Ion Mass Spectrometry (ToF-SIMS) and X-ray Photoelectron Spectroscopy (XPS) was developped. In addition, inductively coupled plasma mass spectrometry (ICP-MS) was used to quantify the total mass of sorbed metal on the nanoplastics.

This innovative analytical approach from the top surface to the core of nanoplastics demonstrated not only the interactions with copper at the surface level, but also the ability of nanoplastics to absorb metal at their core. Indeed, after 24 h of exposition, the copper concentration at the nanoplastic surface remained constant due to saturation whereas the copper concentration inside the nanoplastic keeps

increasing with the time. The sorption kinetic was evaluated to increase with the density of charge of the nanoplastic and the pH. This study confirmed the ability of nanoplastics to act as metal pollutant carriers by both adsorption and absorption phenomena.

Keywords: Nanoplastics, metal sorption, XPS, ToF-SIMS, ICPMS.

Introduction

Plastics, due to their high demand in everyday usage, have been tremendously manufactured in the whole world since the 1950's. The quantity produced increases year after year and results in an important generation of waste. Around 10% of plastics are thrown away and hence found accumulated in the aquatic systems (Koelmans and Kalčíková, 2019).

Characteristics such as low density, good mechanical properties, strong resistance to external stress and low cost have contributed to the success of plastic materials in our daily lives. The problem with this type of waste is that they tend to fragments into smaller pieces *i.e.* micro and nanoplastics (MPTs and NPTs) through mechanical (Ekvall et al., 2019), photodegradation (Lambert and Wagner, 2016), chemical degradation, or biodegradation (Dawson et al., 2018).

While microplastics represent particles with a diameter < 5 mm (Hartmann et al., 2019), NPTs are defined as the smallest colloid plastic debris (1-1000 nm) of mixed shape and chemical composition (Gigault et al., 2018). Although the breakdown of plastic waste is certainly the most common source of NPTs, material wear such as synthetic fabrics or car tire abrasion can also lead to environmental NPTs.

NPTs represents an analytical challenge even up to this day due to their small size and low environmental concentration (Mitrano et al., 2021). Currently, NPTs can be detected in several environmental compartments, such as air (Masry et al., 2021), soil (Wahl et al., 2021), freshwater (Zhang et al., 2021), oceans (Ter Halle et al., 2017) and biota (Kukkola et al., 2021) but not quantified. However, it is presumed that due to their intrinsic properties, NPTs will have a greater impact onto biota. Indeed, unlike microplastics, which may be stuck in living organisms, NPTs will pass biological barriers (e.g. the gut epithelium) and enter the body of species (Grodzicki et al., 2021).

In addition, their small size implies a high surface-area-to-volume ratio, (Oriekhova and Stoll, 2018), which is expected to increase their toxicity throughout the ab/adsorption and transport of chemical co-pollutants such as trace metals or persistent organic pollutants (POPs) (Wagner and Lambert, 2018). The interaction of different trace metals with environmental micro- or NPTs has already been demonstrated mostly using metal in their higher oxidation states as Pb^{2+} (Davranche et al., 2019; Pessoni et al., 2019), Cu^{2+} (Bellingeri et al., 2019), Ag^{2+} (Domenech et al., 2021) in different environmental conditions. Furthermore, NPTs porosity, surface area, and polarity continue to grow due to aging, enabling a stronger interaction with metals (Turner and Holmes, 2015). Indeed, the generation of oxygen containing groups at NPT surface during weathering promotes the adsorption of hydrophilic pollutants such as metallic ions (Mao et al., 2020). Finally, when studying the roles of NPTs as metal vectors, several environmental factors influencing the rate and concentration of pollutant should be considered, including the surface chemistry of NPTs, the pH of the medium and the exposure time (Zou et al., 2020).

Most of the aforementioned studies were focused on the evaluation of the kinetic of adsorption or the adsorption capacity of MPTs or NPTs by the mean of classical isotherms theory. Nevertheless, to our knowledge, the evaluation of the sorption of metallic ions both at the surface and the core of a NPTs has not yet been studied. Such comportment could increase the preconcentration of pollutants by the NPTs and thus accentuate their ability to act as a vector of pollutant.

The aim of the present study was to assess the interactions between NPTs and copper at both the surface and core scale. The diffusion coefficient of metal species within plastic polymer bodies was evaluated to be extremely slow in comparison with those applicable for metal ions in bulk aqueous media (Town et al., 2018).

There has been an increasing concern over the combined toxic effects of microplastics, NPTs and metallic pollutants on aquatic organisms due to their intrinsic interaction. Copper has often been chosen as target

analyte because as trace metal it is ubiquitous and persistent in the environment. It is found in all aquatic compartments due to anthropogenic inputs as organic agriculture. If copper remains an essential trace element for organisms, excessive doses can induce toxic effects (Hoang et al., 2009). Studied performed on different species pointed out the negative influence of NPTs to environmental species through their interaction with copper (Bellingeri et al., 2020; Gao et al., 2022; Machado et al., 2021; Wan et al., 2021).

In this work, NPT model materials of polystyrene have been elaborated free of surfactants and preservatives to avoid any bias of interpretation (Pikuda et al., 2019) and with a functionalized surface mimicking the oxidized environmental samples. The interaction mechanisms between these NPT model materials and copper were studied at the surface scale using two surface analysis techniques: Time-of-Flight Secondary Ion Mass Spectrometry (ToF-SIMS) and X-ray Photoelectron Spectroscopy (XPS). The former was chosen to evaluate the elemental and molecular composition at the extreme surface (1-2nm) of NPTs, while the latter was used to quantitatively characterize the chemical composition of the NPTs surface (5-10nm). In addition, inductively coupled plasma mass spectrometry (ICP-MS) was used to quantify the total mass of the sorbed metal on NPTs.

Materials and Methods

Materials. Acrylic Acid (AA ≥ 99%), styrene (S ≥ 99%), ammonium persulfate (APS ≥ 99%), copper (II) nitrate hydrate ($Cu(NO_3)_2$), nitric acid (HNO_3) (Sigma-Aldrich), sodium hydroxide pellets (NaOH) (ABCR) were used as received without further purification unless noted. Deionized water, with a resistivity of 18.2 MΩ cm^{-1} at 25°C, was filtered through a 0.22 µm Millipore filter prior to use.

Synthesis of NPT material models. Styrene / acrylic acid copolymer nanoparticles were elaborated by a soap-free copolymerization process using APS as initiator. The detailed procedure of polymerization is reported elsewhere (Pessoni et al., 2019).

All the reactions were performed at 70 °C under nitrogen atmosphere with a mechanical stirring at 350 rpm. The recipe for the copolymerization process is listed in Table S1. The NPT suspension was purified by at least 5 cycles of centrifugation-dispersion in deionized water at 12 000 rotation per min during 30 min until the supernatant conductivity is equal to that of deionized water.

Microscopy. The morphology of the NPT models were investigated by scanning electron microscopy (SEM) using a Hirox SH-3000 with a 25 kV accelerated voltage. Atomic Force Microscope (AFM) images were recorded using an AFM MultiMode8® from Brucker©, on peak force mode.

Surface area. The surface area was computed with the BET theory (Brunauer et al., 1938) applied on the N_2 adsorption isotherm measured at 77 K on the Micromeritics® Tristar II 3020. Even if the surface area computed are small, the criterion of Rouquerol *et al.* (Rouquerol et al., 2007) was used to accurately select the range of relative pressures for the calculation of the specific surfaces. The surface area occupied by a N_2 molecule at 77 K was taken as $\sigma = 16.2$ Å^2.

Titration. The titration measurements were performed on a Titrando 888 equipped with a stirrer 728 and a combined pH glass electrode (pH: 0-14; 0-80°C; KCl: 3 M). All components were purchased from Metrohm. The software used was Tiamo 2.5. The pH of the nanoparticle aqueous solution (1000 mg L^{-1}) was increased to 10 with a 0.1M NaOH solution, then carboxylate functions were titrated using a 0.5x10-3 M HCl solution. The supernatant was titrated using a 0.1M NaOH solution.

Copper and NPT exposure. A stock solution of NPTs (80000 mg L^{-1}) and a stock solution of copper (40000 mg L^{-1}) prepared by solubilizing copper (II) nitrate crystals into ultrapure water were used to prepare 40000 mg L^{-1} NPT dispersion with a copper concentration of 2000 mg L^{-1}. The pH was adjusted to 5 by using a 1 M NaOH solution. The Cu/NPTs mixture was then left under stirring for 24 to 144 hours at room temperature. The mixtures were then purified by centrifugation at 15000 rpm during 30 min, the supernatant was collected to be analyzed by ICPMS whereas the pellet (NPTs with copper sorbed) was

redispersed in an equal volume of deionized water. This process of centrifugation, removal of the supernatant and replacement by an equal volume of deionized water was reproduced two extra times. After 3 cycles of centrifugation less than 3 % of residual copper was measured by ICPMS in the supernatant (**Figure S6**). 50 µL of the washed mixture was deposited by drop casting onto a 10 mm² silica wafer cleaned beforehand by UV/ozone exposition during 15 min to be analyzed by XPS and ToF-SIMS.

XPS. X-Ray Photoelectron Spectroscopy (XPS) measurements were performed on a Thermo K-alpha spectrometer equipped with a focused monochromatized Al-Kα radiation (hγ=1486.6 eV). Core ionization peaks were recorded with a 20 eV constant pass energy (PE) over an ellipsoidal area of 200 x 400 µm. Charge effects were compensated by the use of a dual-beam charge neutralization system (low energy electrons and ions). Data treatment was performed with CasaXPS software. Peak fitting was processed with a non-linear Shirley-type background and mathematical components are obtained by a weighted least-squares calculation method using 30 % Lorentzian and 70 % Gaussian line shapes. Spectral calibration was done based on the C1s component at 285 eV binding energy, attributed to C-C/C-H environment. Quantifications were calculated using Scofield's relative sensitivity factors corrected by - 0.6 in intensity.

ToF-SIMS. ToF-SIMS analysis were carried out using a TRIFT V nanoToF II (Physical Electronics, Chanhassen (MN), US) equipped with a 30 kV Bi-LMIG. All mass spectra were acquired at room temperature using the same experimental conditions, so that to perform semi-quantitative analysis (comparing the ratio of peaks intensities). For surface analysis ("bunched" mode, best mass resolution), the LMIG gun was tuned to deliver Bi_3^{++} bismuth clusters primary ions with a dc current of 12 nA over a 50 µm raster size; the mass range was fixed between 0 and 2000 uma and the number of frames was set to 50 (dose: 5.4 $x10^{12}$ ions/cm^2) for both polarities. For 2D imaging ("unbunched" mode, best spatial resolution), a resolution of 256x256 image pixels, with a time per channel of 128, over 50x50 μm^2 field-of view was used and the

PIDD (primary ion dose density) never exceeded the static limit of 2.10^{13} ion.cm^{-2}. Dual beam (15 eV e^- /10eV Ar^+) charge compensation system was used for all analyses. Data processing was performed using ToF-DR software provided by Physical Electronics. All positive polarity mass spectra were calibrated using CH^+ (m/z = 13), CH_2^+ (m/z = 15) and Na^+ (m/z 23) peaks and all negative polarity mass spectra were calibrated considering CH^+(m/z = 13), C_2H^+ (m/z = 15) and OH^- (m/z = 17) peaks.

ICPMS. An Agilent 7900 ICPMS (Agilent, Tokyo, Japan) was used to determine the total copper content in the supernatant by monitoring isotopes ^{63}Cu and ^{65}Cu. The system consists of an integrated auto-sampler, a concentric nebulizer and a quartz cyclonic spray chamber as a sample introduction system. Each sample was analyzed by triplicate. Results are expressed as the mean of three measurements.

Copper sorption. The equilibrium copper concentration in the supernatant was determined by ICPMS. The sorbed amount of copper Q_{sorb} (mg g^{-1}) was determined according to the equation 1 where C_0 is the initial copper concentration (mg L^{-1}), C_e is the residual copper concentration in the supernatant (mg L^{-1}) of the first centrifugation step (see "Copper and NPT exposure" part), V is the total volume of the solution (L) and m is the total NPT mass (g). The theoretical maximum of sorption $Q_{e,max}$ is obtained when $C_e = 0$.

$$Q_{sorb}\ (mg\ \ g^{-1}) = \frac{(C_0 - C_e)V}{m}$$

Equation 1

Environmental NPTs concentration is estimated to be at ppt range, however, without appropriate sampling methods and sample treatment, underestimations of actual environmental concentrations should not be excluded. Moreover, environmental concentration of both NPTs and pollutant vary over time and spatiotemporal hotspots are more than probable. In our work, we decided to perform the sorption experiment at relatively high NPTs concentrations considering the aforementioned remarks, i.e. 40000 mg L^{-1} and the samples have been exposed to 2000 mg L^{-1} of copper. Such experimental conditions

were necessary to favor sorption kinetics and being at a laboratory experiment time scale. Additionally, these experimental concentrations were expected to allow both phenomena, *i.e.* adsorption and absorption to occur while low concentration would very preferably to adsorption due to the stronger interaction forces on the surface.

Results and discussion

Nanoplastics material models synthesis and characterization.

The soap-free process involves the copolymerization of a hydrophobic and a hydrophilic monomer. The latter may be both polymerized and located either within the core or at the surface of the polymer particles during their elaboration process. Only the part of it present at the latex particle surface provides particle stability in water (Ceska, 1974).

Acrylic acid (AA) and styrene (S) were used in this work as hydrophilic and hydrophobic monomers respectively. Beyond providing stability to the particles, the use of a carboxylic acid monomer as AA allows to reproduce the surface oxidation occurring in environmental condition (Fotopoulou and Karapanagioti, 2012; ter Halle et al., 2017). Two batches have been synthesized and named PS9 and PS22; they differ from the carboxylic content, *i.e.* the former was obtained with a monomer molar ratio AA/S = 0.09 while the second latter corresponds to a molar ratio AA/S = 0.22. After polymerization in water dispersed medium and purification, the NPTs were characterized in terms of size and size dispersity.

The polydispersity index (PDI) values of the samples were lower than 0.05 suggesting a narrow size distribution *i.e.* monodisperse NPTs. The average particle size was measured in aqueous solution using DLS; PS22 and PS9 exhibit a diameter size of 330 and 350 nm, respectively. This slight difference of particle size can be explained by the initial acidic monomer content in the polymerization feed. Indeed, a higher AA/S molar ratio results in the nucleation of more primary particles. As the concentration of monomer is

fixed in both synthesis, the number of monomer units per nanoparticle decreases and therefore the size of latex particles is reduced (Polpanich et al., 2005)

The surface morphology has been characterized by SEM and AFM (Figure 1). PS9 and PS22 are spherical particles differing from each other by their roughness as confirmed by AFM measurement. A smooth surface with few defects was observed for the PS9 sample, while a rough surface assimilated to a raspberry-like morphology was observed for the PS22.

Additionally, the specific surface of both samples was determined using the Brunauer-Emmett-Teller (BET) method (**Figure S1**). As expected, the sample with a smooth surface (PS9) shows a lower specific surface, with a value of 15 $m^2\ g^{-1}$ for PS9, while a specific surface of 29 $m^2\ g^{-1}$ was obtained for the sample PS22. The higher surface area of PS22 sample in comparison to that of PS9 is in agreement with a difference of roughness between the two samples as observed by AFM. The specific surface area for PS9 is close to the one theoretically calculated considering a solid and smooth sphere (16 $m^2\ g^{-1}$), while the experimental result is twice as high as the theoretical one for the PS22 (17 $m^2\ g^{-1}$).

The number of carboxylic functions by mean surface area (Equation 2) is obtained by dividing the amount of acid groups by the surface area (measured by BET) of the titrated particles while the number of carboxylic functions by grams of particles was obtained by dividing the number of titrated groups by the mass of particles (Equation 3).

$$[COOH](mol/nm^2) = \frac{n_{COOH}}{S_{Spec.} \times (\frac{m}{V \times \rho_{sty}})}$$

Equation 2

$$[COOH](mol/g) = \frac{n_{COOH}}{m}$$

Equation 3

Where n_{COOH} (mol) is the number of carboxylic groups obtained by titration, S_{spec} ($nm^2\ g^{-1}$) is the specific surface determined by BET measurement, m (g) is the mass of NPTs, V is the volume of NPTs (cm^3), ρ_{sty} ($g\ cm^{-3}$) is the density of polystyrene given at 1,04 $g\ cm^{-3}$.

PS22 and PS9 surface functionality reach respectively 24 COOH groups per nm^2 (1.15 $mmol_{COOH}\ g^{-1}$) and 5 COOH/nm^2 (0.11 $mmol_{COOH}\ g^{-1}$).

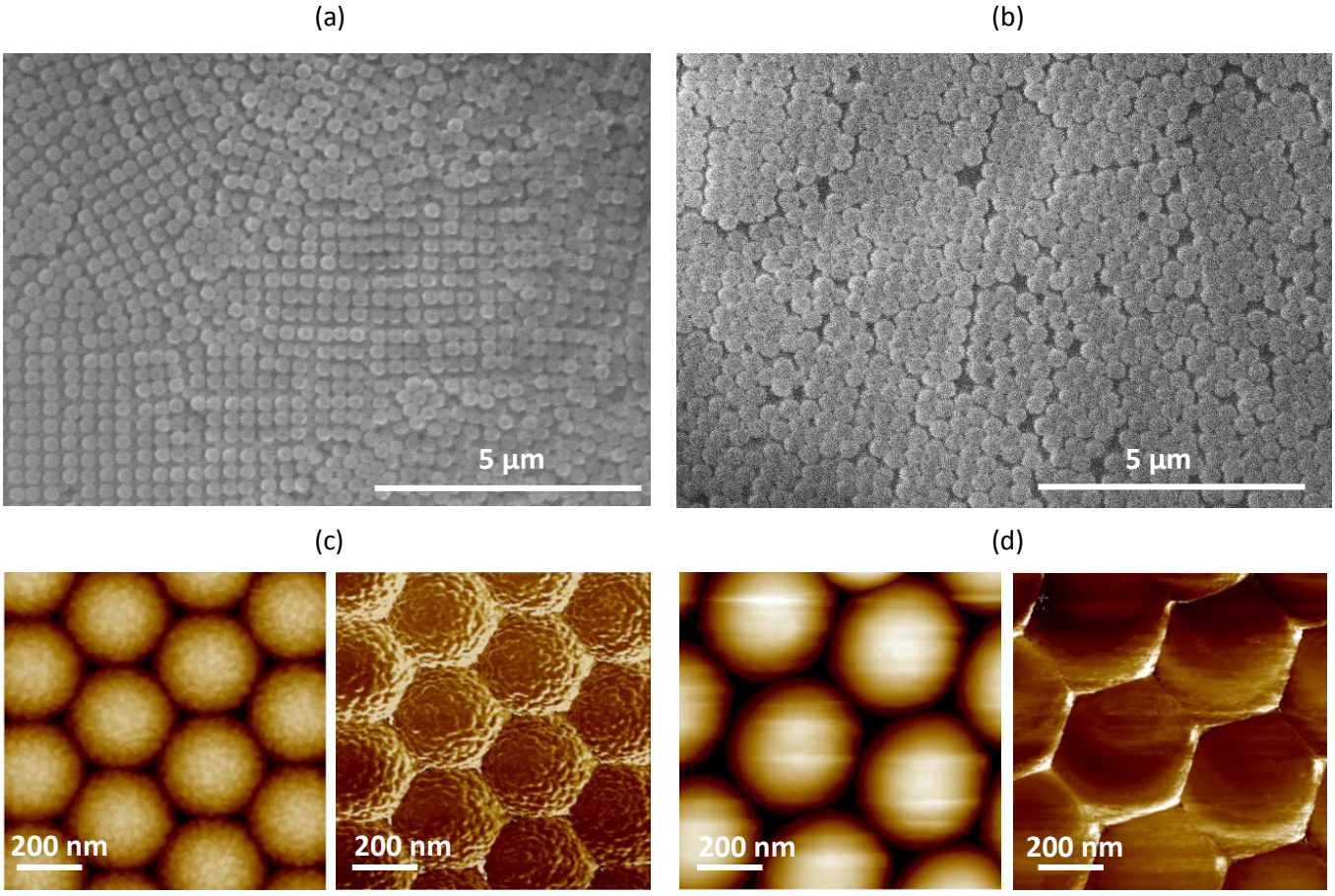

Figure 1. First line: SEM images of a NPT film (a) PS22, (b) PS9 ; Second line Peak Force mode AFM images, height profile (left), deformation profile (right) of the NPT film : (c) PS22 and (d) PS9.

Exposure to copper. The interaction between NPTs with a carboxylic functionalized-surface and copper was investigated at pH of 3 and 5. If, a higher pH may appear to be more relevant to environmental conditions, those conditions have been chosen to favor the NPTs/copper interaction. Indeed, the literature reports pKa of 4.1 and 4.5 respectively for the acrylic acid monomer and the poly(acrylic acid), respectively (Michaels and Morelos, 1955; Wiśniewska and Chibowski, 2005) and ionic copper is in

complexed form above pH 5 (Cuppett, 2006). Working from pH 3 to 5 ensures to keep copper under its free ionic state and to have partially to predominantly negatively charged carboxylate groups at the NPTs surface at the same time, thus favoring the interaction phenomena study. The effect of the surface carboxylic group content is evaluated onto sorption mechanism as an image of the effect of the surface oxidation *i.e.* aging of plastic debris. After an exposure time ranching from 24 to 144 hours, the samples were analyzed by TOF SIMS and XPS to characterize the surface chemical composition from 1-2 nm up to 10 nm depth respectively, and by ICPMS to determine the copper content of the whole NPTs. Therefore, the differences between surface and bulk analysis results allows us to determine the copper adsorbed at the extreme surface and the copper absorbed by the whole NPTs.

Surface analysis of NPTs before copper exposure. In order to quantitatively characterize the surface of NPTs, the two batches of NPT models (PS9 and PS22) were analyzed by XPS before exposition to copper. The main elements detected at the surface of the two NPT models were carbon and oxygen as shown by the full scan survey spectrum (**Figure S2**). The C1s spectra highlights the presence of 4 types of carbon at ~~a~~ binding energies of 285 eV, 285.8 eV, 289.5 eV and 291.6 eV, respectively assigned to **C**-**C**/**C**-H, C-**C=**O, O-**C=**O and π- π* (Table. 1). Both the C-CO and COO bindings are characteristics of the AA units.

These data confirm the presence of acid groups at the surface of the NPT models. The proportions of **C**O, **C**OO and **O**=C, **O**-C are higher for PS22 (8.8 at.% and 7.9 at.%) compared to PS9 (1.9 at.% and 2.2 at.%), which confirms a higher density of carboxylic groups at the surface of the former and highlights the influence of the initial AA content in the feed during the synthesis. These results also confirm XPS as a technique able to provide quantitative chemical information of NPT surface.

Table 1. XPS quantitative analysis for PS22 and PS9 samples.

Region	Be (eV)	FWHM (eV)	%at. Conc		Assignment
			PS22	PS9	
C1s	285.0	1.3	65.3	81.6	C-C / C-H
	285.8	1.3	8.8	1.9	CO
	289.5	1.5	8.8	1.9	COO
	291.6	1.3	1.3	5.6	π- π*
O1s	533.5	1.8	7.9	2.2	O=C
	533.9	1.8	7.9	2.2	O-C

Surface analysis of NPTs after copper exposure. Quantitative and qualitative surface chemical composition of S/AA NPTs exposed to a copper solution was achieved by combining XPS and ToF-SIMS measurements.

X-ray Photoelectron Spectroscopy (XPS)

In addition to carbon and oxygen, after exposure copper was clearly identified as one of the main elements present at the surface of the NPT model materials on the XPS survey spectra **(Figure S3).**

The XPS C1s, O1s and Cu2p high-resolution spectra of NPTs exposed to copper for 24 h are presented in Erreur ! Source du renvoi introuvable**.** The C1s core peak shows no difference in chemical environment with the results obtained before exposition.

The 4 types of carbon, C-C/C-H at 285eV, C-CO at 285.8 eV, COO at 289.5 eV and π- π* at 291.6 eV, are still present with similar proportions. Also, no difference in the C1s chemical environment was noted as a function of either the incubation time within the copper solution (Erreur ! Source du renvoi introuvable. **and Figure S4**) or the pH of the solution (pH= 3 or 5) (Erreur ! Source du renvoi introuvable.). Such results confirm the absence of any bond between copper and carbon atoms that would have modified the carbon spectra.

Contrary to the C1s core peak, the O1s core peak shows a new component at a higher binding energy (532.0 eV) after copper exposition, which is assigned to the oxygen bound to copper metal O-Cu. This component is observed whatever the exposition time or the pH of the solution, but its atomic percentage (presented in the **Table 2**) is clearly different depending on the type of NPTs and the pH with the following tendency $PS22_{(pH5)} > PS9_{(pH5)} > PS22_{(pH3)} > PS9_{(ph3)}$. Indeed, the atomic percent of O-Cu for the PS22 sample is measured at 4.5 and 0.8 % at pH 5 and 3 respectively while it is only 1.1 and 0.5 % for the PS9 at pH 5 and 3 respectively which proves the influence first of the pH and second of the carboxylic groups proportion on the interaction with copper.

The Cu 2p core peak shows two main peaks assigned to Cu $2p_{3/2}$ and Cu $2p_{1/2}$ components due to the spin-orbit coupling. Each peak can be deconvoluted into two components at 933.5 / 935.0 eV and 953.1 / 954.7 eV respectively, which are characteristics of a mixture of Cu(I) and Cu(II) species. In addition, the presence of a shake-up satellite specific to the presence of Cu(II) species is also observed (Pauly et al., 2014), more predominantly for pH 5. It is noted that the atomic percentage of Cu is more important at pH 5 compared to pH 3 and for PS22 compared to PS9, which is in agreement with the results obtained for O1s.

Regarding the XPS quantitative analysis at different exposure times : 24 h (**Table 2**) ; 48 h (**Table S2**) and 144 h (**Table S3**), two results can be highlighted:

1) At the same exposure time, the adsorbed copper concentration increases both with the carboxylic acid surface density and the pH ($PS22_{(ph5)} > PS9_{(ph5)} > PS22_{(pH3)} > PS9_{(ph3)}$). Indeed, PS22 sample exposed to copper for 24 h exhibits anatomic % of Cu 2p component of 4.6 at pH 5 while it is only 0.9 at pH 3. Similarly, for PS9 sample the measured atomic % is 2.1 at the highest pH and 0.4 at the lowest. Considering carboxylic acid surface groups as the main adsorption sites for copper ions, an increase in carboxylic acid implies the adsorption of more copper. Therefore, the increase of copper concentration for the highest functionalized sample (PS22) is consistent. Considering the pH of exposure, the pKa of PAA is close to 4,

281 therefore at pH 5 the acid groups are predominantly on their basic COO^- form (Michaels and Morelos,
282 1955; Wiśniewska and Chibowski, 2005) and the adsorption of the positively charged Cu^{2+} copper ions is
283 hence favored.. 2) There is no significant variation of copper concentration throughout the different
284 exposure times (24, 48 or 144 hours) whatever the pH value, indicating that the sorption kinetic is high
285 enough to obtain a maximum of adsorption before the first measurement occurring after 24 h of
286 exposure. It can be assumed that in less than a day the NPT surface is saturated with copper.

287

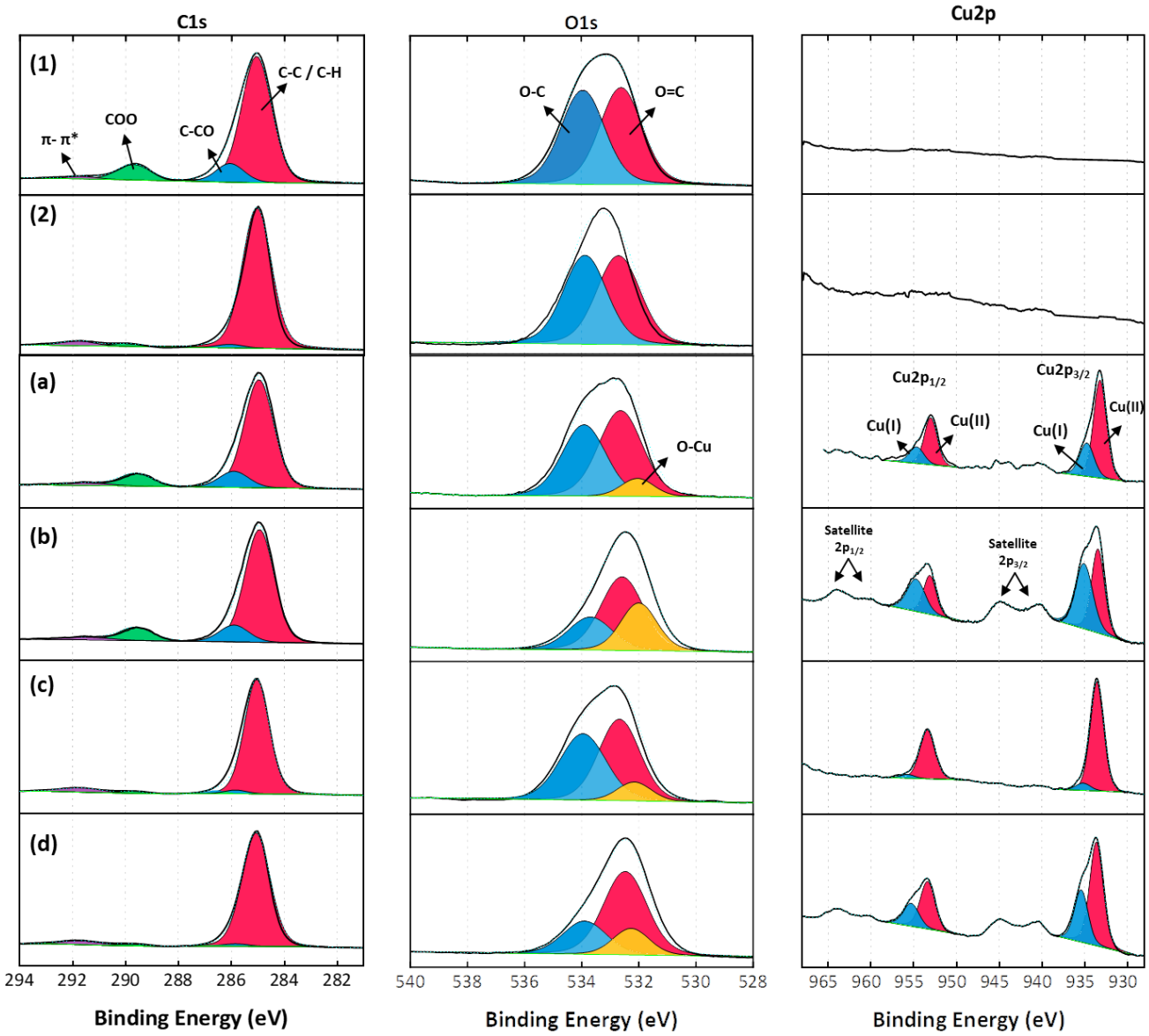

288

289 **Figure 2.** C 1s, O 1s and Cu 2p high resolution XPS spectra of (1) PS22 and (2) PS9 without copper exposure; and of PS22 at (a)
290 pH3, (b) pH5 and PS9 at (c) pH3, (d) pH5 after copper exposure for 24 h, the quantification data can be found in the table 2.

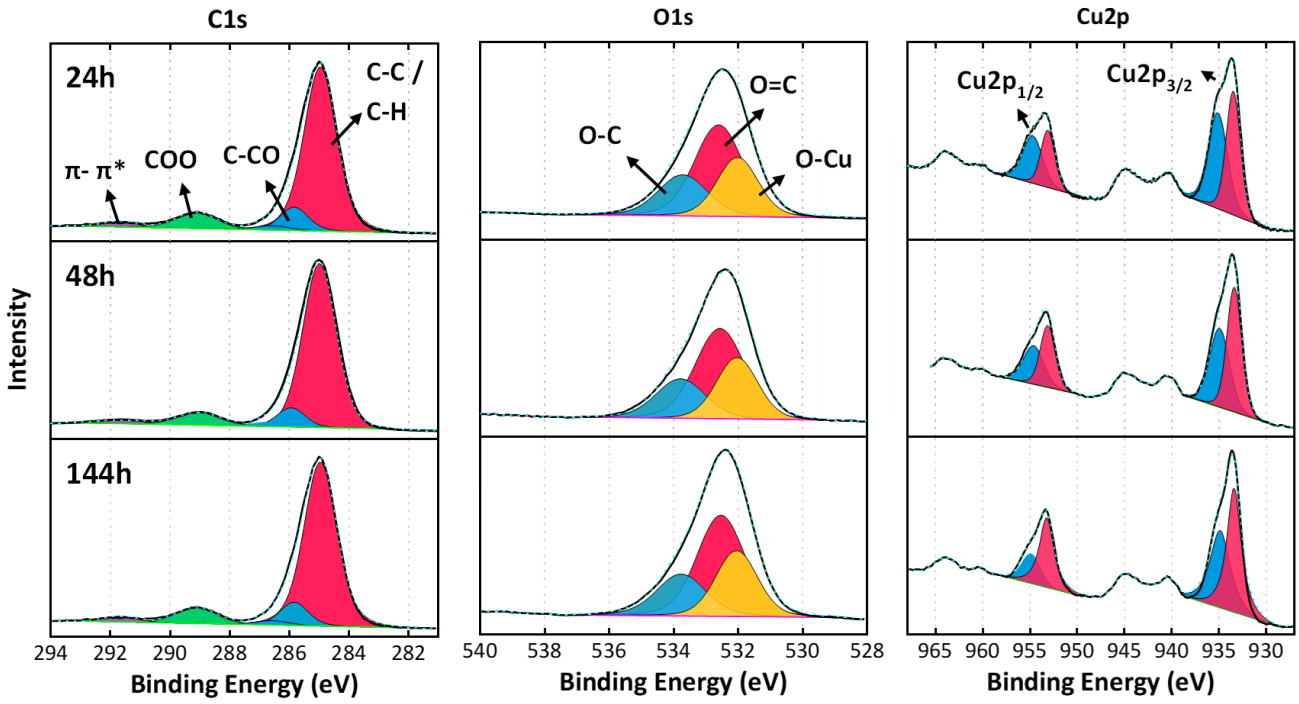

Figure 3. XPS C 1s, O 1s and Cu 2p core peaks of PS22 sample incubated with copper at pH 5 for 24 h (first line), 48 h (second line) and 144 h (third line), the quantification data can be found in the table 2.

Table 2. XPS quantitative analysis of PS22 and PS9 samples exposed for 24h with copper at either pH 5 or 3.

Region	Be (eV)	FWHM (eV)	Assignment	%at. Conc			
				pH = 3		pH = 5	
				PS22	PS9	PS22	PS9
C1s	285.0	1.3	C-C / C-H	61,2	85.0	59.2	84.1
	285.8	1.3	C-CO	9.0	2.2	8.5	2.1
	289.5	1.5	COO	9.0	2.2	8.5	2.3
	291.6	1.3	π- π*	2.5	5.7	2.3	4.1
O1s	533.5	1.8	O=C	8.8	1.8	8.1	2.7
	533.9	1.8	O-C	7.8	2.2	3.5	1.5
	532.0	1.5	O-Cu	0.8	0.5	4.5	1.1
Cu2p	933.5	1.8	$Cu2p_{3/2}$	0.4	0.3	1.4	0.7
	935.0	2		0.2	0.02	1.1	0.5
	953.1	1.8	$Cu2p_{1/2}$	0.2	0.2	1.3	0.6
	954.7	2		0.1	0.02	0.8	0.3

298

299 *Time-of-flight secondary ion mass spectrometry analysis (ToF-SIMS)*

300 **Figure 4** presents the ToF-SIMS mass spectra obtained in positive polarity for PS22 sample after 24h
301 exposure time with copper. Two main peaks at m/z 63 and 65 characteristics of the two copper isotopes
302 $^{63}Cu^+$ and $^{65}Cu^+$ are clearly detected with the expected isotopic ratio. The same result is obtained with the
303 PS9 sample (**Figure S5**). These results confirm the presence of copper at the extreme surface (1-2 nm) of
304 the NPTs after 24h exposure time whatever the surface carboxylic group content. Organic fragments
305 specific of the polymer structure of the NPTs are also observed, such as $C_2H_3^+$, $C_3H_3^+$, $C_6H_5^+$, $C_7H_7^+$ or C_9H_7.
306 More interestingly, oxidized copper molecular fragments like $Cu_2(OH)^+$ and $C_4H_8O_3Cu^+$, as well as C_2HCu^+
307 fragment which comes from the fragmentation of a bigger polymeric molecule associated with Cu, can be
308 identified, confirming the interactions between the NPTs containing carboxylic groups and copper.
309 Moreover, ToF-SIMS 2D chemical imaging of the NPTs surface highlights the spatial distribution of species
310 of interest like Cu^+, $C_2HCu_2^+$ or $C_9H_7^+$ as shown in **Figure 4**. (c), (d) and (e) respectively; the color scale
311 indicated on the side represents the signal intensity, the yellow/white color corresponds to the highest
312 and black one to the lowest. Copper is relatively well dispersed at the surface over the analyzed area at
313 the ToF-SIMS resolution and by comparison with the SEM image (**Figure 4.f**).

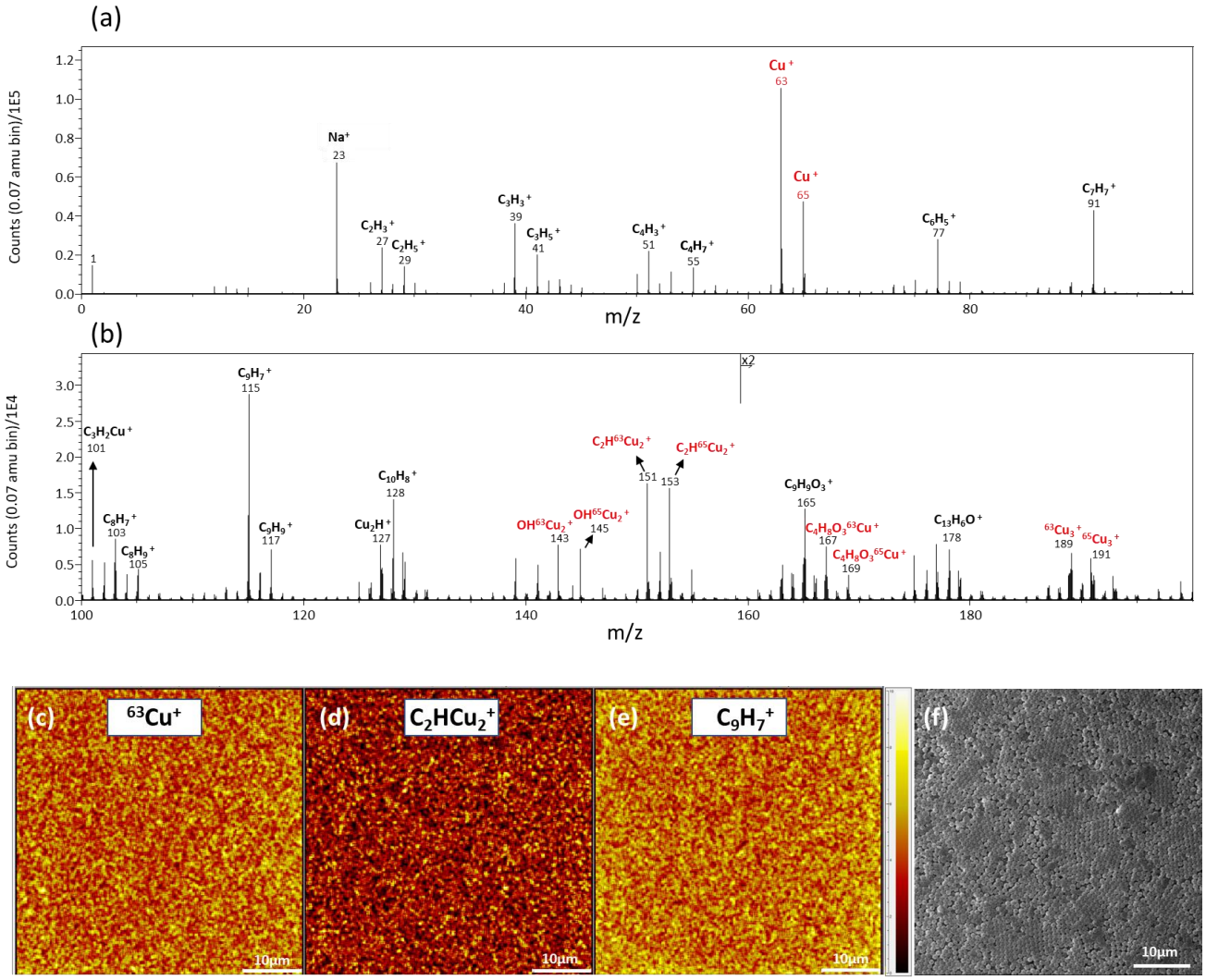

Figure 4. ToF-SIMS surface analysis of PS22 sample after 24h exposure time with copper: positive polarity spectra over m/z range 0 to 100 (a) and 100 to 200 (b); 2D chemical imaging (10 µm scale bar, the color scale represents the signal intensity, yellow/white for the highest and black for the lowest) of : c) 63Cu+ ; d) C2HCu2+ and e) C9H7+ fragments. f) SEM image (10 µm scale bar).

Total copper determination (ICPMS). The free copper fraction (*i.e.* the amount of copper not absorbed/adsorbed onto the NPTs and hence remaining free in the aqueous solution) was quantified by ICPMS. This fraction was collected in the supernatant after centrifugation of the NPT suspension exposed to copper. The fraction of copper sorbed by the NPTs was deduced by subtracting the free copper from the initial concentration of copper in the mixture and is expressed as sorption capacity Q_{sorb} (mg of copper per g of NPT) (**Figure 5** (right).

326 It stands out that, for a similar exposition time, the copper concentration sorbed by the NPTs increases
327 both with the pH and the density of carboxylic sites at the surface. For instance, after 24 h of exposure a
328 sorption capacity of 14.4 and 52.8 mg g^{-1} were obtained for the PS22 sample at pH 3 and 5 respectively,
329 while it's evaluated at 8.8 and 25.1 mg g^{-1} for the PS9 sample at pH 3 and 5 respectively. These results
330 confirm the sorption of copper by NPTs and the role of the carboxylic sites present at the NPTs surface:
331 the more carboxylic groups the more sorbed copper.

332 **Highlighting the diffusion of copper**

333 To evaluate the ability of copper to diffuse in the core of the NPTs, we compared the evolution of the
334 trend (**Figure 5**) between the surface analysis (by XPS: left) and total analysis (surface + core: by ICPMS,
335 right)

336 Unlike the surface analysis, the total copper concentration in the particle increases with the copper
337 exposure time. This is particularly clear for all samples at pH 3 while for PS22 sample at pH 5 the
338 concentration reaches a plateau at 48 h. It is assumed that the latter is due to the fast kinetic of sorption
339 as almost all the copper in the solution was sorbed by the PS22 NPTs after only 24 h of exposure (the
340 theoretical maximum of sorption $Q_{sorb,max}$ is represented by the red line).

341 This trend could not be observed by surface analysis; indeed, the atomic percent of copper at the surface
342 measured by XPS remained quite constant between 24 to 144 h of exposure time regardless of the
343 conditions. Such results suggest that the extreme surface (5-10 nm) of the NPT model materials is quickly
344 saturated in copper, but copper still diffuse inside the NPT with time.

345

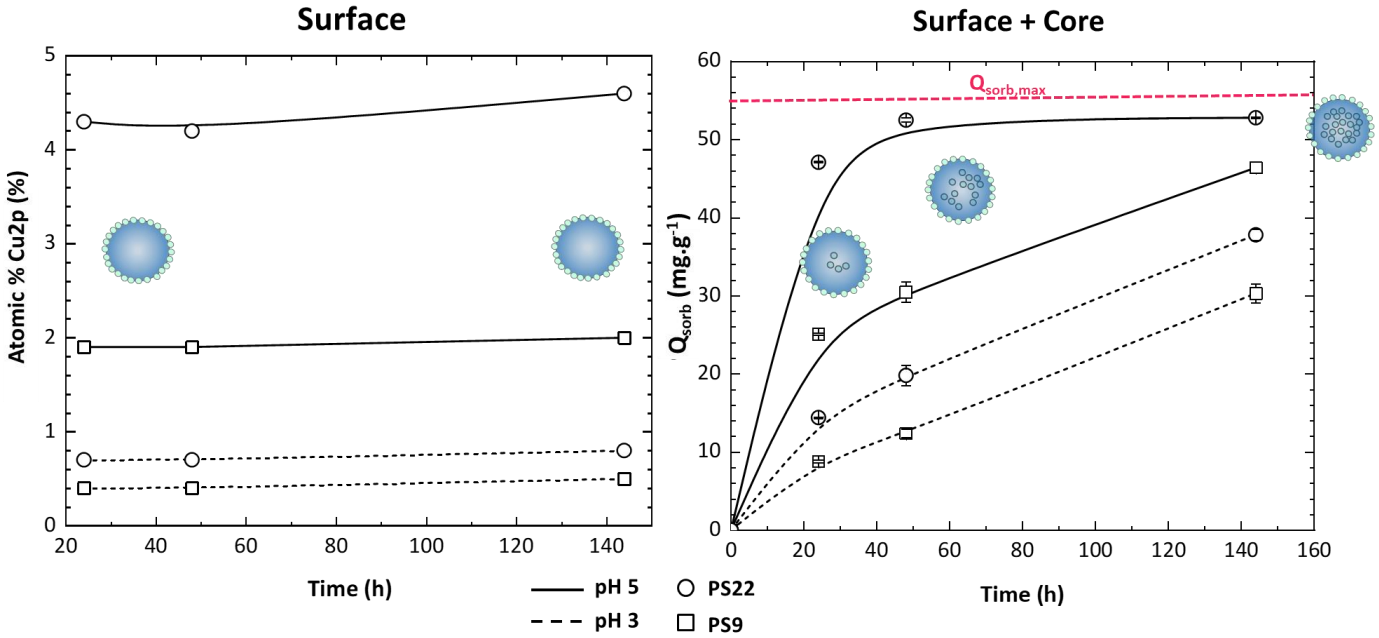

Figure 5. Evolution of the copper atomic percent (left, obtained by XPS)) and the masse sorption capacity (right, obtained by ICPMS) of PS22 and PS9 samples at pH3 and 5; the red line represents the theoritical maximum of sorption.

Conclusion and perspectives In this work, for the first time, two complementary surface techniques (XPS and ToF-SIMS) has been used to study the interactions between copper and NPTs model materials at the extreme surface. XPS has proved to provide both elemental and quantitative information, showing, on the one hand, a significant amount of copper at the NPT surface after 24 h of incubation and, on the other hand, an increase of this amount in direct correlation with the increasing of the functionalization of the NPT surface. In addition, the complementary molecular information obtained by ToF-SIMS confirmed the direct interaction of copper with the carboxylic groups. Finally, the diffusion of copper within the core of a NPT was reported for the first time, by comparing the evolution of the copper concentration at the surface, obtained by XPS, and in the whole NPT materials, obtained by ICPMS. Indeed, the atomic percent of copper measures at the surface of the NPTs remained unchanged regardless of the exposure time whereas the concentration of copper sorbed keeps increasing with the time. In addition, copper sorption rate seems to increase with the carboxylic group content at the NPT surface.

This study confirmed the ability of nanoplastics to act as metal pollutant carriers by both adsorption and absorption phenomena and the phenomenon is more rapid with aged (more oxydized) plastic debris. It should be noted that, the formation of biofilm at the nanoplastics surface in addition to the desorption of the metallic pollutant from the NPTs represents additional parameters that must be taken into account in perspective works.

Conflicts of interest

There are no conflicts of interest to declare.

Acknowledgements

We acknowledge funding and support from the French Agency for Research-ANR (ANR-PLASTI-SCARE)). The funding of the ICP-MS instrument by the AQUITRACES (project n 20131206001-1301097) by Aquitaine Region is acknowledged. We acknowledge PELLERIN Virginie and Seif El Islam Lebouachera for technical support in microscopic and BET surface analysis.

Notes and references

Bellingeri, A., Bergami, E., Grassi, G., Faleri, C., Redondo-Hasselerharm, P., Koelmans, A.A., Corsi, I., 2019. Combined effects of nanoplastics and copper on the freshwater alga Raphidocelis subcapitata. Aquat. Toxicol. 210, 179–187. https://doi.org/10.1016/j.aquatox.2019.02.022

Bellingeri, A., Casabianca, S., Capellacci, S., Faleri, C., Paccagnini, E., Lupetti, P., Koelmans, A.A., Penna, A., Corsi, I., 2020. Impact of polystyrene nanoparticles on marine diatom Skeletonema marinoi chain assemblages and consequences on their ecological role in marine ecosystems. Environ. Pollut. 262, 114268. https://doi.org/10.1016/j.envpol.2020.114268

Ceska, G.W., 1974. The effect of carboxylic monomers on surfactant-free emulsion copolymerization. J. Appl. Polym. Sci. 18, 427–437. https://doi.org/10.1002/app.1974.070180210

Cuppett, J.D., 2006. Evaluation of Copper Speciation and Water Quality Factors That Affect Aqueous Copper Tasting Response. Chem. Senses 31, 689–697. https://doi.org/10.1093/chemse/bjl010

Davranche, M., Veclin, C., Pierson-Wickmann, A.-C., El Hadri, H., Grassl, B., Rowenczyk, L., Dia, A., Ter Halle, A., Blancho, F., Reynaud, S., Gigault, J., 2019. Are nanoplastics able to bind significant

amount of metals? The lead example. Environ. Pollut. 249, 940–948. https://doi.org/10.1016/j.envpol.2019.03.087
Dawson, A.L., Kawaguchi, S., King, C.K., Townsend, K.A., King, R., Huston, W.M., Bengtson Nash, S.M., 2018. Turning microplastics into nanoplastics through digestive fragmentation by Antarctic krill. Nat. Commun. 9, 1001. https://doi.org/10.1038/s41467-018-03465-9
Domenech, J., Cortés, C., Vela, L., Marcos, R., Hernández, A., 2021. Polystyrene Nanoplastics as Carriers of Metals. Interactions of Polystyrene Nanoparticles with Silver Nanoparticles and Silver Nitrate, and Their Effects on Human Intestinal Caco-2 Cells. Biomolecules 11, 859. https://doi.org/10.3390/biom11060859
Ekvall, M.T., Lundqvist, M., Kelpsiene, E., Šileikis, E., Gunnarsson, S.B., Cedervall, T., 2019. Nanoplastics formed during the mechanical breakdown of daily-use polystyrene products. Nanoscale Adv. 1, 1055–1061. https://doi.org/10.1039/C8NA00210J
Fotopoulou, K.N., Karapanagioti, H.K., 2012. Surface properties of beached plastic pellets. Mar. Environ. Res. 81, 70–77. https://doi.org/10.1016/j.marenvres.2012.08.010
Gao, Z., Wang, S., Zhang, Y., Liu, F., 2022. Single and combined toxicity of polystyrene nanoplastics and copper on Platymonas helgolandica var. tsingtaoensis: Perspectives from growth inhibition, chlorophyll content and oxidative stress. Sci. Total Environ. 829, 154571. https://doi.org/10.1016/j.scitotenv.2022.154571
Gigault, J., Halle, A. ter, Baudrimont, M., Pascal, P.-Y., Gauffre, F., Phi, T.-L., El Hadri, H., Grassl, B., Reynaud, S., 2018. Current opinion: What is a nanoplastic? Environ. Pollut. 235, 1030–1034. https://doi.org/10.1016/j.envpol.2018.01.024
Grodzicki, W., Dziendzikowska, K., Gromadzka-Ostrowska, J., Kruszewski, M., 2021. Nanoplastic Impact on the Gut-Brain Axis: Current Knowledge and Future Directions. Int. J. Mol. Sci. 22, 12795. https://doi.org/10.3390/ijms222312795
Hartmann, N.B., Hüffer, T., Thompson, R.C., Hassellöv, M., Verschoor, A., Daugaard, A.E., Rist, S., Karlsson, T., Brennholt, N., Cole, M., Herrling, M.P., Hess, M.C., Ivleva, N.P., Lusher, A.L., Wagner, M., 2019. Are We Speaking the Same Language? Recommendations for a Definition and Categorization Framework for Plastic Debris. Environ. Sci. Technol. 53, 1039–1047. https://doi.org/10.1021/acs.est.8b05297
Hoang, T.C., Schuler, L.J., Rogevich, E.C., Bachman, P.M., Rand, G.M., Frakes, R.A., 2009. Copper Release, Speciation, and Toxicity Following Multiple Floodings of Copper Enriched Agriculture Soils: Implications in Everglades Restoration. Water. Air. Soil Pollut. 199, 79–93. https://doi.org/10.1007/s11270-008-9861-2
Koelmans, B., Kalčíková, G., 2019. A scientific perspective on microplastics in nature and society. SAPEA, Berlin.
Kukkola, A., Krause, S., Lynch, I., Sambrook Smith, G.H., Nel, H., 2021. Nano and microplastic interactions with freshwater biota – Current knowledge, challenges and future solutions. Environ. Int. 152, 106504. https://doi.org/10.1016/j.envint.2021.106504
Lambert, S., Wagner, M., 2016. Formation of microscopic particles during the degradation of different polymers. Chemosphere 161, 510–517. https://doi.org/10.1016/j.chemosphere.2016.07.042
Machado, A.J.T., Mataribu, B., Serrão, C., da Silva Silvestre, L., Farias, D.F., Bergami, E., Corsi, I., Marques-Santos, L.F., 2021. Single and combined toxicity of amino-functionalized polystyrene nanoparticles with potassium dichromate and copper sulfate on brine shrimp Artemia franciscana larvae. Environ. Sci. Pollut. Res. 28, 45317–45334. https://doi.org/10.1007/s11356-021-13907-5
Mao, R., Lang, M., Yu, X., Wu, R., Yang, X., Guo, X., 2020. Aging mechanism of microplastics with UV irradiation and its effects on the adsorption of heavy metals. J. Hazard. Mater. 393, 122515. https://doi.org/10.1016/j.jhazmat.2020.122515

Masry, M., Rossignol, S., Temime Roussel, B., Bourgogne, D., Bussière, P.-O., R'mili, B., Wong-Wah-Chung, P., 2021. Experimental evidence of plastic particles transfer at the water-air interface through bubble bursting. Environ. Pollut. 280, 116949. https://doi.org/10.1016/j.envpol.2021.116949

Michaels, A.S., Morelos, O., 1955. Polyelectrolyte Adsorption by Kaolinite. Ind. Eng. Chem. 47, 1801–1809. https://doi.org/10.1021/ie50549a029

Mitrano, D.M., Wick, P., Nowack, B., 2021. Placing nanoplastics in the context of global plastic pollution. Nat. Nanotechnol. 16, 491–500. https://doi.org/10.1038/s41565-021-00888-2

Oriekhova, O., Stoll, S., 2018. Heteroaggregation of nanoplastic particles in the presence of inorganic colloids and natural organic matter. Environ. Sci. Nano 5, 792–799. https://doi.org/10.1039/C7EN01119A

Pauly, N., Tougaard, S., Yubero, F., 2014. Determination of the Cu 2p primary excitation spectra for Cu, Cu2O and CuO. Surf. Sci. 620, 17–22. https://doi.org/10.1016/j.susc.2013.10.009

Pessoni, L., Veclin, C., El Hadri, H., Cugnet, C., Davranche, M., Pierson-Wickmann, A.-C., Gigault, J., Grassl, B., Reynaud, S., 2019. Soap- and metal-free polystyrene latex particles as a nanoplastic model. Environ. Sci. Nano 6, 2253–2258. https://doi.org/10.1039/C9EN00384C

Pikuda, O., Xu, E.G., Berk, D., Tufenkji, N., 2019. Toxicity Assessments of Micro- and Nanoplastics Can Be Confounded by Preservatives in Commercial Formulations. Environ. Sci. Technol. Lett. 6, 21–25. https://doi.org/10.1021/acs.estlett.8b00614

Polpanich, D., Tangboriboonrat, P., Elaïssari, A., 2005. The effect of acrylic acid amount on the colloidal properties of polystyrene latex. Colloid Polym. Sci. 284, 183–191. https://doi.org/10.1007/s00396-005-1366-6

Ter Halle, A., Jeanneau, L., Martignac, M., Jardé, E., Pedrono, B., Brach, L., Gigault, J., 2017. Nanoplastic in the North Atlantic Subtropical Gyre. Environ. Sci. Technol. 51, 13689–13697. https://doi.org/10.1021/acs.est.7b03667

ter Halle, A., Ladirat, L., Martignac, M., Mingotaud, A.F., Boyron, O., Perez, E., 2017. To what extent are microplastics from the open ocean weathered? Environ. Pollut. 227, 167–174. https://doi.org/10.1016/j.envpol.2017.04.051

Town, R.M., van Leeuwen, H.P., Blust, R., 2018. Biochemodynamic Features of Metal Ions Bound by Micro- and Nano-Plastics in Aquatic Media. Front. Chem. 6, 627. https://doi.org/10.3389/fchem.2018.00627

Turner, A., Holmes, L.A., 2015. Adsorption of trace metals by microplastic pellets in fresh water. Environ. Chem. 12, 600. https://doi.org/10.1071/EN14143

Wagner, M., Lambert, S. (Eds.), 2018. Freshwater Microplastics: Emerging Environmental Contaminants?, The Handbook of Environmental Chemistry. Springer International Publishing, Cham. https://doi.org/10.1007/978-3-319-61615-5

Wahl, A., Le Juge, C., Davranche, M., El Hadri, H., Grassl, B., Reynaud, S., Gigault, J., 2021. Nanoplastic occurrence in a soil amended with plastic debris. Chemosphere 262, 127784. https://doi.org/10.1016/j.chemosphere.2020.127784

Wan, J.-K., Chu, W.-L., Kok, Y.-Y., Lee, C.-S., 2021. Influence of polystyrene microplastic and nanoplastic on copper toxicity in two freshwater microalgae. Environ. Sci. Pollut. Res. 28, 33649–33668. https://doi.org/10.1007/s11356-021-12983-x

Wiśniewska, M., Chibowski, S., 2005. Influence of Temperature and Purity of Polyacrylic Acid on its Adsorption and Surface Structures at the ZrO_2 /Polymer Solution Interface. Adsorpt. Sci. Technol. 23, 655–667. https://doi.org/10.1260/026361705775373279

Zhang, B., Chao, J., Chen, L., Liu, L., Yang, X., Wang, Q., 2021. Research progress of nanoplastics in freshwater. Sci. Total Environ. 757, 143791. https://doi.org/10.1016/j.scitotenv.2020.143791

Zou, J., Liu, X., Zhang, D., Yuan, X., 2020. Adsorption of three bivalent metals by four chemical distinct microplastics. Chemosphere 248, 126064. https://doi.org/10.1016/j.chemosphere.2020.126064